Supporting Information

Shape complementarity processes for ultrashort-burst sensitive M13–PEG–WS_2-powered MCF-7 cancer cell sensors

Maria P. Meivita,[1] Shao-Xiang Go,[1] Fitya S. Mozar,[1] Lunna Li,[2] Yaw Sing Tan,[3] Natasa Bajalovic,[1] Desmond K. Loke[1]

[1]Department of Science, Mathematics and Technology, Singapore University of Technology and Design, Singapore 487372, Singapore

[2]Thomas Young Centre and Department of Chemical Engineering, University College London, London WC1E 7JE, U.K.

*[2]Bioinformatics Institute, Agency for Science, Technology and Research (A*STAR), Singapore 138671, Singapore*

[*]Correspondence and requests for material should be addressed to N.B. (e-mail: natasa_bajalovic@sutd.edu.sg) or D.K.L (e-mail: desmond_loke@sutd.edu.sg).

Table S1. Components of the computed binding free energy (kcal mol^{-1}) for the docked models of the HER2–G3P complex[a]

Model	ΔE_{ele}	ΔE_{vdw}	$\Delta E_{nonpolar}$	ΔE_{polar}	ΔG_{bind}
1	438.8 ± 38.6	-118.9 ± 17.2	-14.6 ± 1.2	-397.1 ± 36.0	-91.8 ± 12.9
3	421.8 ± 23.9	-82.9 ± 6.4	-11.5 ± 0.6	-392.3 ± 21.4	-65.0 ± 4.9
4	388.9 ± 27.3	-100.4 ± 12.5	-14.2 ± 2.0	-348.5 ± 16.6	-74.3 ± 3.9
5	364.8 ± 33.0	-127.0 ± 24.4	-16.6 ± 2.9	-328.3 ± 35.0	-107.2 ± 21.1

[a]ΔE_{ele}, electrostatic potential energy; ΔE_{vdw}, van der Waals potential energy; $\Delta E_{nonpolar}$, nonpolar contribution to solvation free energy; ΔE_{polar}, polar contribution to solvation free energy; $\Delta G_{bind} = \Delta E_{ele} + \Delta E_{vdw} + \Delta E_{nonpolar} + \Delta E_{polar}$, free energy change of binding.

Table S2. Statistical significance analysis of the MCF-7 and MCF-10A cell cytotoxicity at different concentrations (10 – 90%) of (a) WS_2 and (b) PPN compared to control (cells only). The significance was fixed based on the Student's t-test and indicated as * ($p < 0.05$), ** ($p < 0.01$), *** ($p < 0.001$), and **** ($p < 0.0001$). Non-significant results were unmarked.

(a) WS_2		**Concentrations (%)**				
		10	**30**	**50**	**70**	**90**
MCF-7	relative to control		***	***	****	****
MCF-10A	relative to control		**	***	***	****

(b) PPN		**Concentrations (%)**				
		10	**30**	**50**	**70**	**90**
MCF-7	relative to control			***	****	****
MCF-10A	relative to control			*	***	****

Table S3. Electrical properties of the cell-layer/nanostructure model utilized in electric-field simulations.

Material	**Isotropic resistivity (Ω cm)**
SiO_2	1.00×10^{16}
ITO	1.00×10^{-4}
PEG/ M13	0.10
Cell in DMEM	97.66
WS_2	1.52

Table S4. References for Figure S7.

Ref No.	Reference
1	Holford, T. R., Davis, F., & Higson, S. P. (2012). Recent trends in antibody based sensors. Biosensors and Bioelectronics, 34(1), 12-24.
2	Karube, I., & Nomura, Y. (2000). Enzyme sensors for environmental analysis. Journal of Molecular Catalysis B: Enzymatic, 10(1-3), 177-181.
3	Zhou, W., Huang, P. J. J., Ding, J., & Liu, J. (2014). Aptamer-based biosensors for biomedical diagnostics. Analyst, 139(11), 2627-2640.
4	Rashid, J. I. A., & Yusof, N. A. (2017). The strategies of DNA immobilization and hybridization detection mechanism in the construction of electrochemical DNA sensor: A review. Sensing and bio-sensing research, 16, 19-31.

Table S5. References for Figure S8.

Ref No.	Reference	Limit of detection (cells μL^{-1})
1	Garcia, D., Ghansah, I., LeBlanc, J., & Butte, M. J. (2012). Counting cells with a low-cost integrated microfluidics-waveguide sensor. Biomicrofluidics, 6(1).	100
2	Huang, J., Zhu, L., Ju, H., & Lei, J. (2019). Telomerase triggered DNA walker with a superhairpin structure for human telomerase activity sensing. Analytical chemistry, 91(11), 6981-6985.	90
4	Rocha Neto, J. B. M., Soares, A. C., Bataglioli, R. A., Carr, O., Costa, C. A. R., Oliveira Jr, O. N., … & Carvalho, H. F. (2020). Polysaccharide multilayer films in sensors for detecting prostate tumor cells based on hyaluronan-CD44 interactions. Cells, 9(6), 1563.	50
5	Sharon, E., Golub, E., Niazov-Elkan, A., Balogh, D., & Willner, I. (2014). Analysis of telomerase by the telomeric hemin/G-quadruplex-controlled aggregation of Au nanoparticles in the presence of cysteine. Analytical chemistry, 86(6), 3153-3158.	27
5	Fu, A. C., Hu, Y., Zhao, Z. H., Su, R., Song, Y., & Zhu, D. (2018). Functionalized paper microzone plate for colorimetry and up-conversion fluorescence dual-mode detection of telomerase based on elongation and capturing amplification. Sensors and Actuators B: Chemical, 259, 642-649.	20
6	Cheng, X., Liu, Y. S., Irimia, D., Demirci, U., Yang, L., Zamir, L., ... & Bashir, R. (2007). Cell detection and counting through cell lysate impedance spectroscopy in microfluidic devices. Lab on a Chip, 7(6), 746-755.	20
7	Chen, Y. F., Wu, H. W., Hong, Y. H., & Lee, H. Y. (2014). 40 GHz RF biosensor based on microwave coplanar waveguide transmission line for cancer cells (HepG2) dielectric characterization. Biosensors and Bioelectronics, 61, 417-421.	20

Table S6. References for Figure S9.

Ref No.	Reference	Signal contrast (the ratio of the normalized signal of healthy cells to that of cancer cells)
1	Das, D., Shiladitya, K., Biswas, K., Dutta, P. K., Parekh, A., Mandal, M., & Das, S. (2015). Wavelet-based multiscale analysis of bioimpedance data measured by electric cell-substrate impedance sensing for classification of cancerous and normal cells. Physical Review E, 92(6), 062702.	0.45
2	Bolat, G., Vural, O. A., Yaman, Y. T., & Abaci, S. (2021). Polydopamine nanoparticles-assisted impedimetric sensor towards label-free lung cancer cell detection. Materials Science and Engineering: C, 119, 111549.	0.72
3	Zhang, F., Jin, T., Hu, Q., & He, P. (2018). Distinguishing skin cancer cells and normal cells using electrical impedance spectroscopy. Journal of Electroanalytical Chemistry, 823, 531-536.	1
4	Park, Y., Kim, H. W., Yun, J., Seo, S., Park, C. J., Lee, J. Z., & Lee, J. H. (2016). Microelectrical impedance spectroscopy for the differentiation between normal and cancerous human urothelial cell lines: real-time electrical impedance measurement at an optimal frequency. BioMed Research International, 2016.	1

Table S7. References for Figure S10.

Ref No.	Reference	Incubation time (h)	Cell viability (%)
1	Song, Y., He, L., Chen, K., Wang, M., Yang, L., He, L., ... & Zhang, Z. (2020). Quantification of EGFR and EGFR-overexpressed cancer cells based on carbon dots@ bimetallic CuCo Prussian blue analogue. RSC advances, 10(47), 28355-28364.	24	75
2	Yang, Y., Fu, Y., Su, H., Mao, L., & Chen, M. (2018). Sensitive detection of MCF-7 human breast cancer cells by using a novel DNA-labeled sandwich electrochemical biosensor. Biosensors and Bioelectronics, 122, 175-182.	24	84.5
3	Tran, H. L., Dega, N. K., Lu, S. M., Huang, Y. F., & Doong, R. A. (2022). Ultrasensitive detection of breast cancer cells with a lectin-based electrochemical sensor using N-doped graphene quantum dots as the sensing probe. Sensors and Actuators B: Chemical, 368, 132233.	24	85
4	Khan, F., Akhtar, N., Jalal, N., Hussain, I., Szmigielski, R., Hayat, M. Q., ... & Janjua, H. A. (2019). Carbon-dot wrapped ZnO nanoparticle-based photoelectrochemical sensor for selective monitoring of H_2O_2 released from cancer cells. Microchimica Acta, 186, 1-9.	24	92

Table S8. References for Figure S11.

Ref No.	Reference	Reading time (ms)
1	Sun, P., Niu, K., Du, H., Li, R., Chen, J., & Lu, X. (2022). Sensitive electrochemical biosensor for rapid screening of tumor biomarker TP53 gene mutation hotspot. Biosensors, 12(8), 658.	50
2	Gholivand, M. B., Ahmadi, E., & Mavaei, M. (2019). A novel voltammetric sensor based on graphene quantum dots-thionine/nano-porous glassy carbon electrode for detection of cisplatin as an anti-cancer drug. Sensors and Actuators B: Chemical, 299, 126975.	50
3	Park, Y., Hong, M. S., Lee, W. H., Kim, J. G., & Kim, K. (2021). Highly sensitive electrochemical aptasensor for detecting the VEGF165 tumor marker with PANI/CNT nanocomposites. Biosensors, 11(4), 114.	50
4	Ruiyi, L., Fangchao, C., Haiyan, Z., Xiulan, S., & Zaijun, L. (2018). Electrochemical sensor for detection of cancer cell based on folic acid and octadecylamine-functionalized graphene aerogel microspheres. Biosensors and Bioelectronics, 119, 156-162.	20
5	Pothipor, C., Wiriyakun, N., Putnin, T., Ngamaroonchote, A., Jakmunee, J., Ounnunkad, K., ... & Aroonyadet, N. (2019). Highly sensitive biosensor based on graphene–poly (3-aminobenzoic acid) modified electrodes and porous-hollowed-silver-gold nanoparticle labelling for prostate cancer detection. Sensors and Actuators B: Chemical, 296, 126657.	20
6	Dai, Y., Abbasi, K., DePietro, M., Butler, S., & Liu, C. C. (2018). Advanced fabrication of biosensor on detection of Glypican-1 using S-Acetylmercaptosuccinic anhydride (SAMSA) modification of antibody. Scientific Reports, 8(1), 13541.	16.7
7	Heller, L., Todorovic, V., & Cemazar, M. (2013). Electrotransfer of single-stranded or double-stranded DNA induces complete regression of palpable B16. F10 mouse melanomas. Cancer gene therapy, 20(12), 695-700.	5

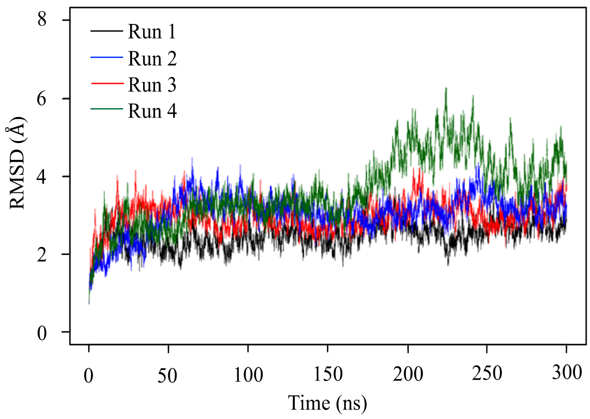

Fig. S1. Root-mean square deviation of Cα atoms in MD simulations of the best-docked model of the G3P–HER2 complex.

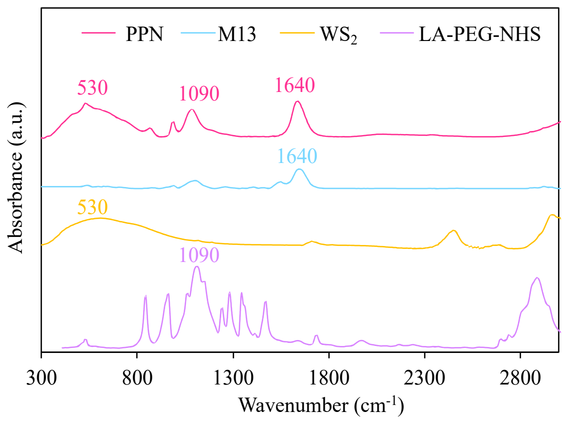

Fig. S2. Fourier transform infrared (FTIR) spectra of the WS_2, LA–PEG–NHS, M13, and PPN.

Other research group's material samples exhibit an FTIR spectrum with an absorption band at 1090 cm^{-1} due to the C-O-C stretching in the PEG, which indicates surface alteration.[1,2] Our material samples generated a similar spectrum, indicating that our results are consistent.

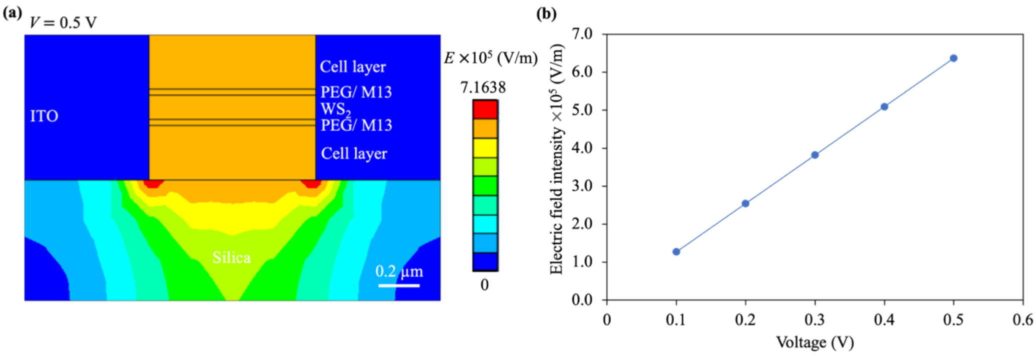

Fig. S3. a) Electric field distribution of the cell-layer/nanostructure model. The WS_2 and PEG/M13 was inserted in the middle of the cell layer, and a square-based reading stimulus was applied. **b)** Variation of the peak electric field in the cell layer for different reading amplitudes.

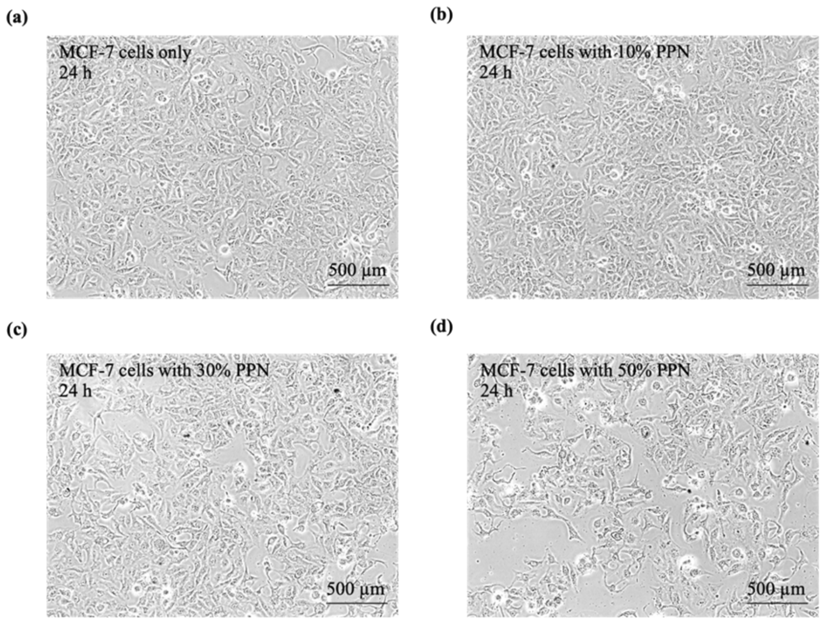

Fig. S4. Microscopy images of MCF-7 cells incubated with **a)** 0%, **b)** 10%, **c)** 30%, and **d)** 50% PPNs for 24 h.

For pristine cells and cells with a low PPN concentration, i.e., MCF-7 cells only and MCF-7 cells with 10% PPNs, the experiments disclose that the nanosheets can exhibit a low extent of cytotoxicity. In contrast, for cells with a high PPN concentration, viz., MCF-7 cells with 30% and 50% PPNs, when the material is added to the cells, the cytotoxicity of the nanosheet, which is connected with the surface process, can result in cell death above a specified amount, leading to a high extent of cytotoxicity.

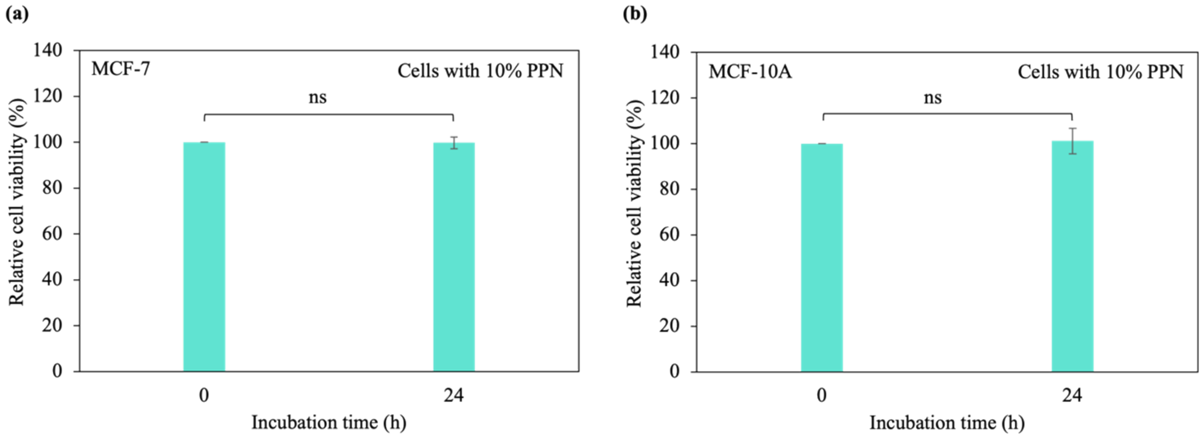

Fig. S5. Variation of the normalized viability of **a)** MCF-7 and **b)** MCF-10A cells incubated with 10% PPN for different times. The significance values were calculated using the Student's t-test and were indicated as follows: non-significant (ns). Data are expressed as the standard error of the mean (SEM), where $n = 6$.

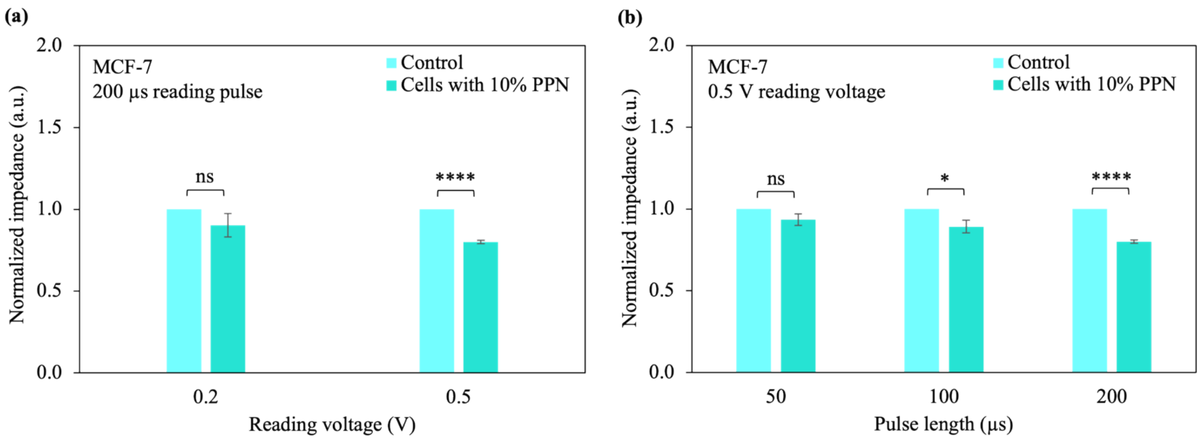

Fig. S6. a) Variations of the normalized impedance for different reading voltages. The cell population was fixed at 7×10^3 cells. **b)** Normalized impedance variation of the P–DBS for different reading lengths. The significance values were calculated using the Student's t-test and were indicated as follows: non-significant (ns), $p \leq 0.05$ (*), and $p \leq 0.0001$ (****). Data are expressed as the standard error of the mean (SEM), where $n = 6$.

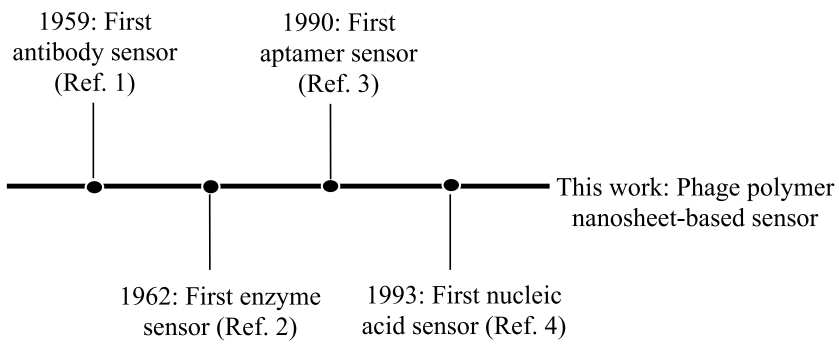

Fig. S7. Timeline of electrical-based cancer cell sensor development. The information for the references can be found in Table S4.

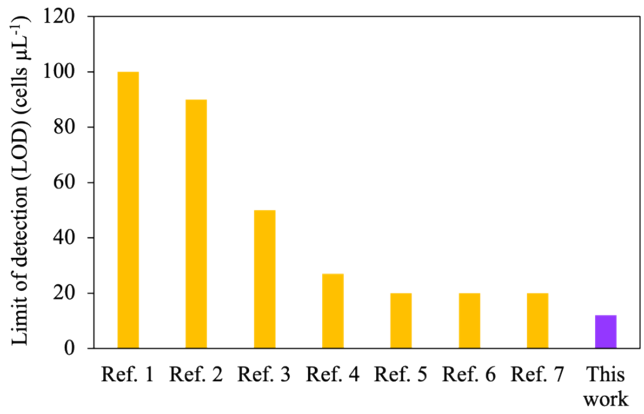

Fig. S8. Comparison of the limit of detection of the P–DBS with that of current sensing methods. The information for the references can be found in Table S5.

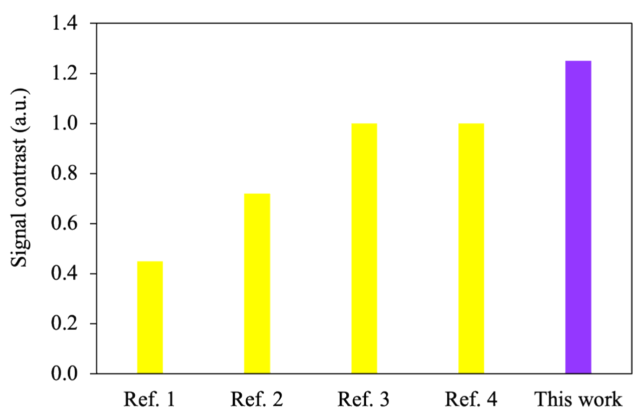

Fig. S9. Comparison of the contrast between the cancer cell sample signal and the healthy cell sample signal of the P–DBS with that of current sensing systems. The information for the references can be found in Table S6.

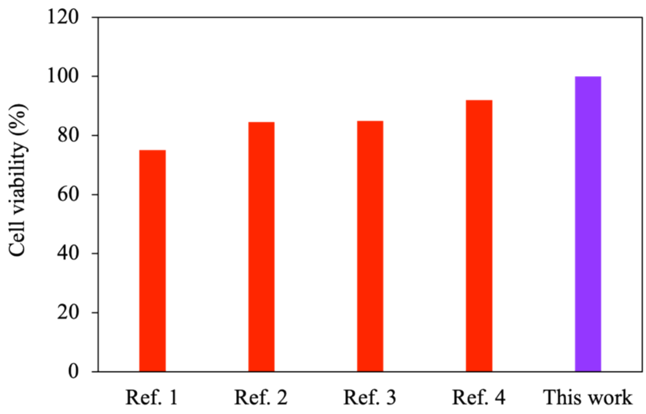

Fig. S10. Comparison of the viability of MCF-7 or MCF-10A cells with the PPN with that of current cancer cells with electrical sensor-based nanostructures. The information for the references can be found in Table S7.

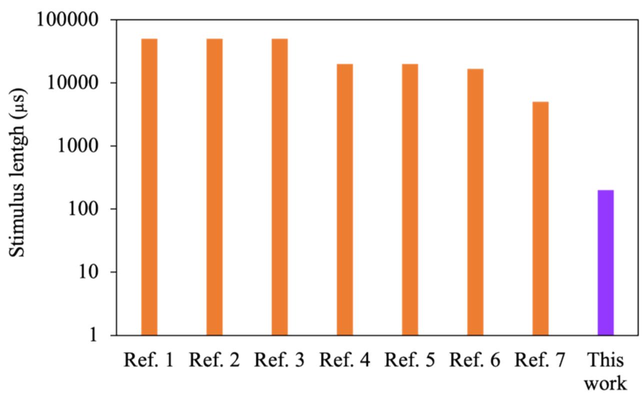

Fig. S11. Comparison of the reading length of the P–DBS with that of current sensing methods. The information for the references can be found in Table S8.

References

1 I. M. Deygen and E. V. Kudryashova, *Colloids Surf. B Biointerfaces*, 2016, **141**, 36–43.
2 A. Kumar, M. Omar Shaikh, R. K. Rakesh Kumar, K. Dutt, C.-T. Pan and C.-H. Chuang, *Nanoscale*, 2022, **14**, 1742–1754.